

Carbon-doped flower-like Bi₂WO₆ decorated carbon nanosphere nanocomposites with enhanced visible light photocatalytic degradation of tetracycline

Xiaona Jiang¹, Shuai Chen¹, Xinrui Zhang¹, Lanni Qu¹, Houjuan Qi¹, Bin Wang^{2,3}, Benbin Xu⁴, and Zhanhua Huang¹, *

¹ Key Laboratory of Bio-based Material Science and Technology, Ministry of Education, College of Material Science and Engineering, Northeast Forestry University, Harbin, 150040, China

² College of Materials Science and Engineering, Taiyuan University of Science and Technology, Taiyuan, 030024, China

³ Advanced Materials Division, Engineered Multifunctional Composites (EMC) Nanotech LLC, Knoxville, TN, 37934, USA

⁴ Mechanical and Construction Engineering, Faculty of Engineering and Environment, Northumbria University, Newcastle Upon Tyne, NE1 8ST, UK

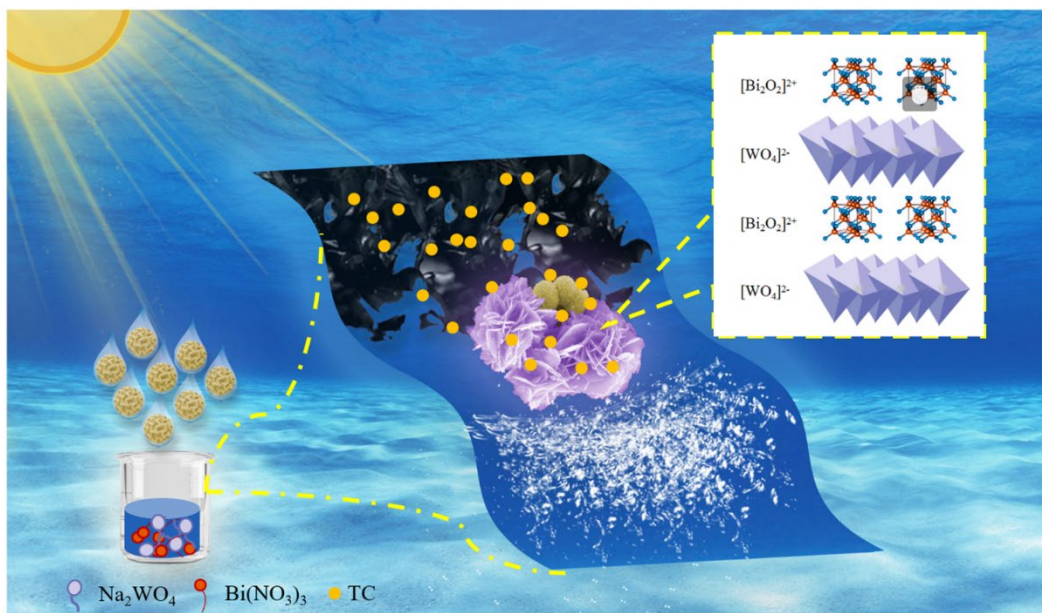
***To whom correspondence can be made**

E-mail: huangzh1975@163.com (Z. H.)

Abstract

In search of a recyclable catalyst with synergistic adsorption and photocatalysis, unique composite photocatalysts of flower-like bismuth tungstate (Bi_2WO_6) and carbon nanospheres (CSs) were composited using a hydrothermal synthesis method (named CSs- Bi_2WO_6). Notably, based on the high visible light utilization and a reasonable band gap (2.53 eV), CSs- Bi_2WO_6 have good photocatalytic properties. For example, the composite with an optimized ratio (2% CSs- Bi_2WO_6) showed good adsorption and photocatalytic performance. Under simulated natural light conditions, the degradation rate of tetracycline (TC) by 2% CSs- Bi_2WO_6 was 84.6% in 60 min, which is nearly 25% higher than pure Bi_2WO_6 . After five cycles, the observed barely decreased TC degradation rate of 2% CSs- Bi_2WO_6 confirmed the high cyclability and reproducibility of the photocatalyst. The total organic carbon estimation of the post-degradation reaction medium corresponded to 68.2% mineralization. Furthermore, we determined the photocatalytic reaction path by LC-MS, which confirmed that the composite catalyst could effectively degrade TC molecules into small molecules. It can be concluded that the catalyst has a broad application prospect in the field of wastewater treatment.

Keyword: Flower-like Bi_2WO_6 , Carbon nanospheres, Synergistic effect, Wastewater treatment, Degradation pathways



Graphical abstract: Carbon-doped Bi_2WO_6 composite catalyst was used to degrade TC in wastewater efficiently

1. Introduction

With the acceleration of global industrialization, environmental pollution has brought serious and inevitable questions to human life [1-5]. The polluted water seeps into the ground, which further leads to different degrees of pollution of soil and groundwater [6, 7]. Therefore, environmental remediation is a necessary task for human beings to survive on Earth. In the past few decades, antibiotics have been diffusely used in the field of biological disease control. Among them, TC has high efficiency in the inhibition and even removal of a variety of pathogenic bacteria, ranking second in the list of global antibiotic production and consumption [8, 9]. Because TC has a stable aromatic ring molecular structure, it is difficult to degrade under natural conditions, which is easy to increase the resistance of receptors, and then threaten human health [10, 11]. Therefore, it is critical to develop efficient and cost-effective methods to control TC in the environment.

Among many methods of sewage treatment, adsorption is considered to be one of the key methods to alleviate water pollution due to its high efficiency and recyclability [12]. We note that the applications of carbon materials in supercapacitors, energy storage, drug delivery, and especially catalysis are widely concerned [13-15]. Since the carbon component can provide high specific surface area and a high visible light utilization, which will effectively enhance the absorption of visible light. In addition, they can also form strong interfacial electronic effects with semiconductors [16, 17], which play a positive role in improving the degradation performance of catalysts. In general, the easy stacking of most carbon materials in the preparation process is an important reason that affects the material properties. Therefore, the preparation of uniform and

stable carbon materials is our key research topic. On the other hand, carbon materials can only adsorb pollutants in the environment and cannot be mineralized into small molecules, thus producing secondary pollution, which limits their adhibition [18, 19]. To solve the problems we mentioned, a strategy of combining adsorption and photocatalysis was proposed: the pollutants are enriched on the surface of carbon materials, and it was further decomposed and mineralized by photocatalysts into small molecules [20, 21].

In recent years, research on photocatalysis technology in energy conversion and environmental remediation has been in full swing [22, 23]. Many Bi-based photocatalysts have been modified by carbonaceous materials [24, 25]. Bi_2WO_6 is one of the semiconductor materials with environmental protection, high light stability, and nontoxicity. Due to its special sandwiches-like layered structure of $[\text{Bi}_2\text{O}_2]^{2+}$ and $[\text{WO}_6]^{2-}$, Bi_2WO_6 has a better optical property and stability than monolayer catalysts [26]. The valence band of Bi_2WO_6 is formed by the hybridization of Bi 6s orbital and O 2p orbital, and the W 5d orbital also constitutes the conduction band in the meantime [27-29]. It shows a suitable band gap value (2.75 eV) and visible light response range for photocatalytic reactions [30]. It is becoming one of the most promising photocatalysts. However, as a result of the fast recombination rate of photogenerated e^- and h^+ , the application of pure Bi_2WO_6 photocatalyst is greatly limited [31]. According to many reports, we have noted that carbon materials have the function of capturing and transporting photogenerated electrons, thus improving photocatalytic performance. For instance, Li et al. [32] modified the Bi_2WO_6 material with carbon materials, and the results showed that the degradation rate of TC (20 mg/L) was 87% in 70 min. Cai et al. reported a direct S-scheme electron transfer mechanism in CZS/CDs/BWO

composite with carbon dots as the electron bridge, which exhibited a wider absorption wavelength compared to the pristine Bi_2WO_6 [33]. Similarly, other photocatalysts based on Bi_2WO_6 composite with carbon materials, such as CDs/Cl- Bi_2WO_6 [34], SCFs/BWO [35], BWO QDs/MCNOs [36], and $\text{Bi}_2\text{WO}_6/\text{rGO}$ [37] were found to exhibit photocatalytic degradation. The above studies have well proven its excellent photocatalytic activity.

In this paper, the composite photocatalyst of CSs- Bi_2WO_6 was prepared by hydrothermal synthesis. It is worth noting that the high dispersion of CSs avoids the aggregation and stacking of catalysts. Moreover, the photocatalytic performances of CSs- Bi_2WO_6 with different proportions have been measured by the photodegradation of TC solution, which presented greatly enhanced photocatalytic activity compared with pure Bi_2WO_6 . The composite catalyst has an excellent photocatalytic degradation effect. Furthermore, according to the intermediate substances produced in the degradation process, a possible photodegradation mechanism driven by visible light was proposed.

2 Experiment section

2.1 Chemicals and Characterization

Detailed information on experimental reagents and characterization was provided in the supporting information.

2.2 Preparation of CSs

CSs were prepared by conventional methods [38], 4 g of D-(+) -glucose was added to 30 mL of deionized water. After stirring for 30 min, the mixture was transferred to a 50 mL Teflon-lined steel autoclave and heated to 180 °C for 8 h. The black - brown carbonaceous material obtained by the hydrothermal reaction was washed three times by centrifugation with water and ethanol, respectively. Finally, the centrifuged products were dried in an oven at 80 °C for 6 h.

2.3 Preparation of CSs-Bi₂WO₆

Bi₂WO₆ were prepared according to the hydrothermal procedure as described elsewhere [39]. In short, about 0.5 mol of Bi(NO₃)₃ · 5H₂O and 0.5 mol Na₂WO₄ · 2H₂O were dissolved in 25 mL of ethylene glycol and stirred to produce a white precipitate. The CSs were dissolved in 10 mL distilled water and then sonicated for 10 min, which was then added dropwise to the above solution. The mixture was then transferred to a Teflon-lined and heated at 140 °C for 14 hours. The samples obtained were washed three times with ethanol and deionized water respectively and then centrifuged. The repeatedly washed sediment was dried at 60 °C. The composite catalysts with

different CSs contents were labeled as Bi_2WO_6 , 0.5% CSs- Bi_2WO_6 , 1% CSs- Bi_2WO_6 , 2% CSs- Bi_2WO_6 , 4% CSs- Bi_2WO_6 , 8% CSs- Bi_2WO_6 .

2.4 Photocatalytic TC degradation

Details of photocatalytic TC degradation are provided in the supporting information.

2.5 Adsorption kinetics study

Details of adsorption kinetics are provided in the supporting information.

3 Results and discussion

3.1 Morphology and structures

Fig. 1a shows that Bi_2WO_6 is a typical ‘flower-like’ structure with a diameter of 3-4 μm . It consists of a large number of nanosheets that cross over and come together to form a 3D structure. As we can see from Fig. 1b, CSs and Bi_2WO_6 are interconnected. However, CSs were clustered on the surface of Bi_2WO_6 , and the end is easier to be covered [40]. The primary reason for this special structure may be that the Bi_2WO_6 sheet is stacked at one end and the stress distribution on the three-dimensional structure surface is not uniform. The structure and morphology of the prepared CSs are shown in Fig. 1c, from which we can find that the CSs is a uniform and well-dispersed nanospheres with an average diameter of about 450 nm. The particle size distribution was shown in Fig. S1 in supporting information. The surface of CSs in Fig. 1b changed from smooth to rough, which may be affected by the growth of Bi_2WO_6 [41]. It could not prevent the CSs from forming close contact with Bi_2WO_6 to form a ‘flower-spheres’ structure, and will even be more conducive to the surface adsorption of organic pollutants. However, if the content of CSs increases, it is easy to form large clusters. This will affect the interaction between CSs and Bi_2WO_6 . The EDS results in Fig. 1d-1g demonstrates the distribution of C, O, W, and Bi elements in the CSs- Bi_2WO_6 composites, indicating the successful production of the composite catalysts.

In Fig. 1h, it can be seen that the 2% CSs- Bi_2WO_6 composite structure exhibits the ‘flower-spheres’ morphology. The layered structure of Bi_2WO_6 can be seen in the picture as consisting of a large number of nanosheets. The CSs are attached to the nanosheets. The TEM image of pure

Bi_2WO_6 and the magnified structure of the 2% CSs- Bi_2WO_6 in Fig. 1h were shown in supporting information (Fig. S2). Fig. 1i shows the HRTEM image of Bi_2WO_6 . We observed lattice fringes of 0.27 nm and 0.32 nm matched perfectly with the (020) and (131) crystal faces of Bi_2WO_6 , which proved the successful synthesis of Bi_2WO_6 [42]. The HRTEM image (Fig. 1j) depicts the good crystallization of 2% CSs- Bi_2WO_6 nanoparticles but an amorphous structure for CSs [43]. The above indicated that the composite catalyst was successfully prepared.

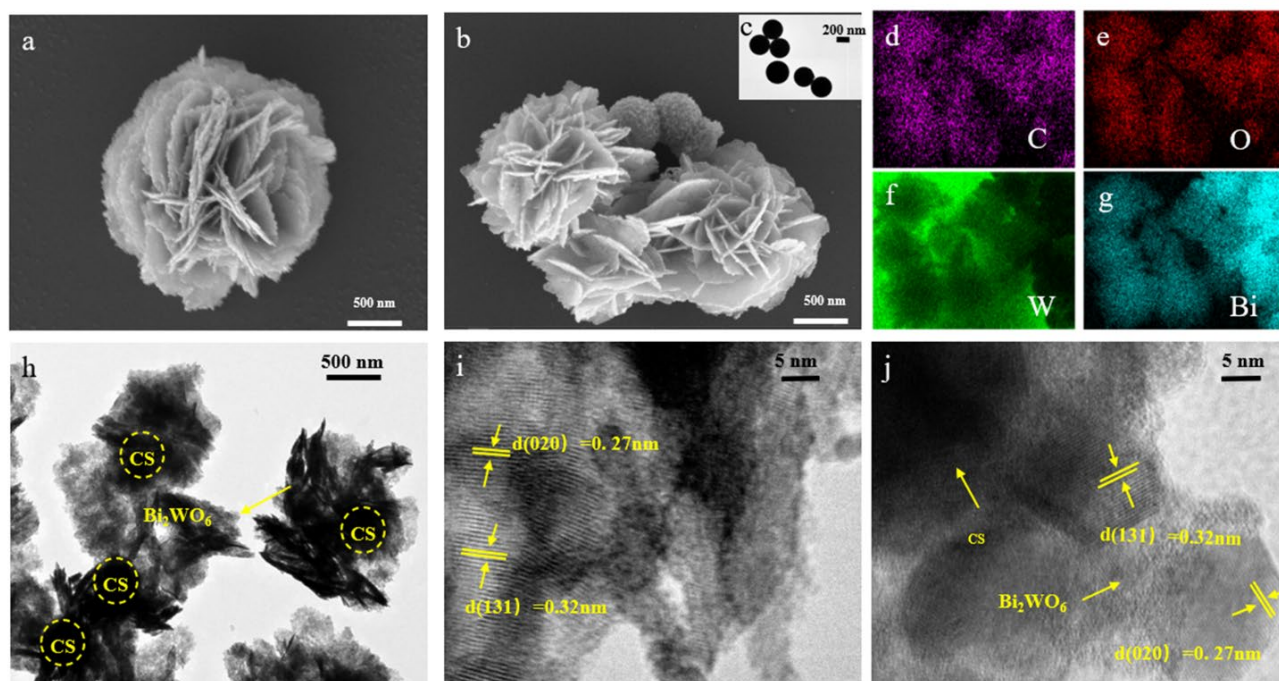


Fig. 1 SEM images of Bi_2WO_6 (a), 2% CSs- Bi_2WO_6 (b), CSs (c), the element distribution of C, O, Bi, and W in 2% CSs- Bi_2WO_6 (d-g), TEM images of 2% CSs- Bi_2WO_6 (h), and HRTEM images (i, j) of Bi_2WO_6 and 2% CSs- Bi_2WO_6

The XRD patterns showed the phase structure of the CSs- Bi_2WO_6 complexes in different proportions (Fig. 2a). The crystal plane (131), (020), (220), (313), (226), (400), (333), and (406) correspond to the characteristic diffraction peaks $2\theta = 28.14^\circ, 32.76^\circ, 47.03^\circ, 55.76^\circ, 58.44^\circ, 68.79^\circ, 75.91^\circ, \text{ and } 78.24^\circ$, respectively. These peaks are sharp and clear as well as matched well with Bi_2WO_6 standard card (PDF#26-1044), demonstrating the successful preparation of Bi_2WO_6

[44, 45]. Fig. S3 further showed the XRD image of CSs. It exhibited a broad peak at around $\sim 44^\circ$, corresponding to (101) reflections of carbon materials. In the XRD pattern of the composite, the diffraction peak of the amorphous structure of CSs phase was not found. This is to some extent expected because of the low crystallinity of amorphous carbon and the incorporation of trace carbon materials during the preparation [46].

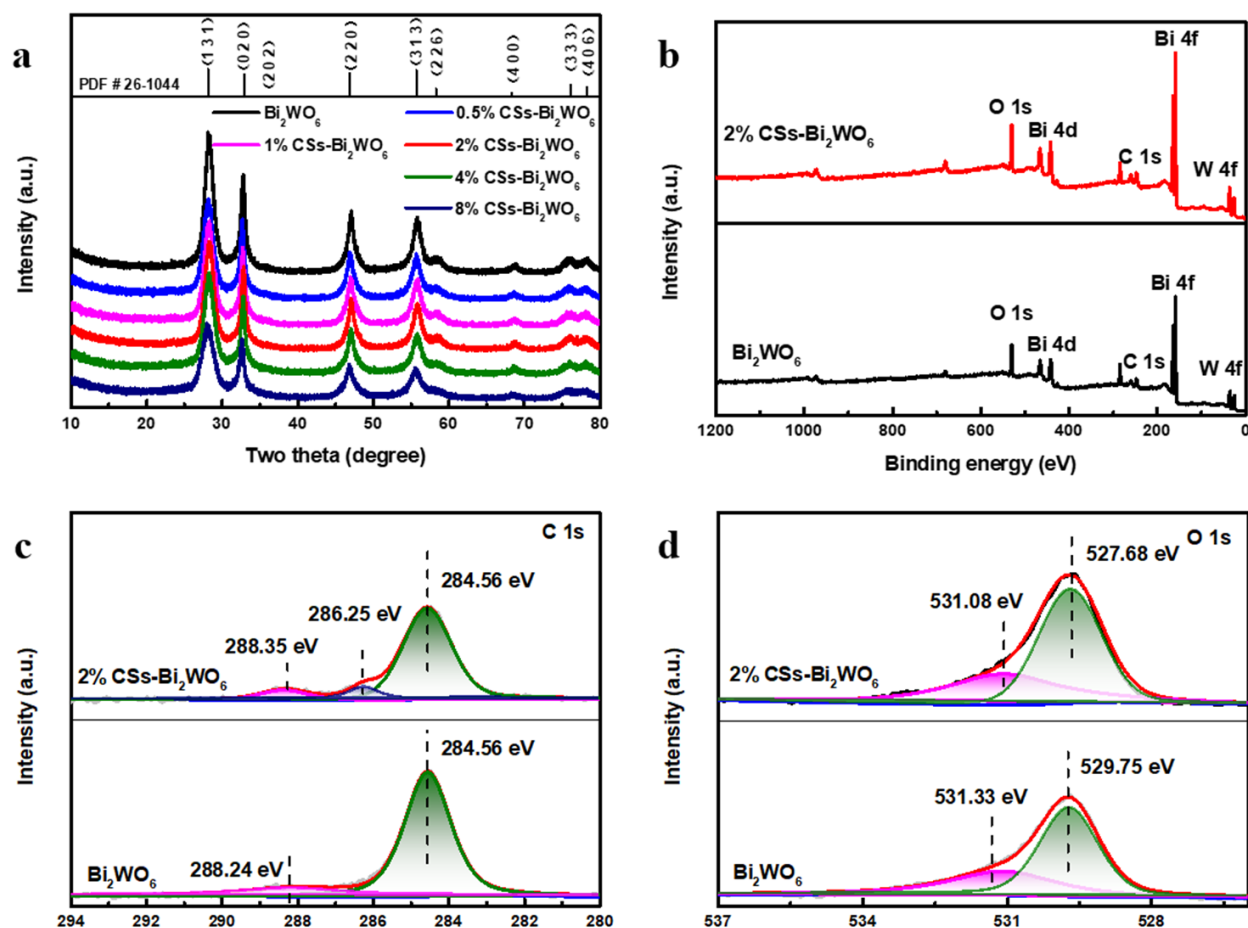


Fig. 2 XRD patterns of Bi_2WO_6 and $\text{CSs-Bi}_2\text{WO}_6$ photocatalysts (a), XPS spectra of the Bi_2WO_6 and 2% $\text{CSs-Bi}_2\text{WO}_6$ (b), C 1s (c), O 1s (d)

The chemical states of Bi_2WO_6 and 2% $\text{CSs-Bi}_2\text{WO}_6$ were analyzed by XPS. Fig. 2b shows the existence of elements C, O, Bi, and W in the sample. The elements of Bi and W peaks were found in supporting information of Fig. S4. Fig. 2c shows C 1s peak for pure Bi_2WO_6 and 2% CSs-

Bi_2WO_6 . All elements' binding energy was calibrated with C 1s of aliphatic carbon at 284.60 eV. The C 1s peak at around 288.24 eV of Bi_2WO_6 was attributed to the adsorbed CO_2 on the surface [47]. The slight shift of C 1s peak at 288.35 eV was speculated of 2% CSs- Bi_2WO_6 to be caused by C = O bond generated by the introduction of BCs. Notably, 2% CSs- Bi_2WO_6 shows a new peak at 286.2 eV, which may be due to the formation of C - O - C between Bi_2WO_6 and CSs (O atom in Bi_2WO_6). The above result indicated that most of C in 2% CSs- Bi_2WO_6 was sp^2 hybridized. The presence of oxygen-containing functional groups in the 2% CSs- Bi_2WO_6 system suggests that the strong interaction between Bi_2WO_6 and carbon nanospheres is formed during the hydrothermal reaction.

As shown in Fig. 2d, the asymmetric peak centered of O 1s at 530 eV was decomposed into two components at the binding energy of 529.74 eV and 531.33 eV for pure Bi_2WO_6 , which were due to the surface lattice oxygen and the adsorbed oxygen species respectively [48, 49]. With the addition of the CSs, the binding energy shifts from 529.75 eV, 531.33 eV (Bi_2WO_6) to 531.08 eV, 527.68 eV (2% CSs- Bi_2WO_6). The peaks of O 1s of 2% CSs- Bi_2WO_6 shifted to the lower binding energy compared to Bi_2WO_6 , indicating the electron cloud density and electronegativity around O decrease due to the addition of carbon spheres. the interactions between Bi_2WO_6 and BCs in the composite [50, 51].

Nitrogen sorption measurements evaluated the surface area and pore structural properties in Fig. 3. In Fig. 3a, the isotherm curves belonged to type IV with H3 hysteresis loops [43, 52, 53]. And specific surface area of pure Bi_2WO_6 , 0.5% CSs- Bi_2WO_6 , 1% CSs- Bi_2WO_6 , 2% CSs- Bi_2WO_6 , 4% CSs- Bi_2WO_6 , and 8% CSs- Bi_2WO_6 was 20.76, 82.45, 84.80, 84.88 85.04 and 82.31 $\text{m}^2 \text{g}^{-1}$,

respectively. Obviously, the addition of surface area was mainly caused by the surface folds of CSs, which will increase the contact area of CSs with contaminants. Interestingly, the surface area of the complex actually decreased when an excess of CSs was introduced. This may be due to the fact that with the increase of CSs, the packing of Bi_2WO_6 became dense, the specific surface area decreased slightly, and the active site decreased [54, 55]. This proves that adsorption is strongly related to the specific surface area of the composite catalyst. The pore size distribution is shown in Fig. 3b, the pore size of samples is almost distributed from 1 nm - 20 nm. Furthermore, the slit-shaped pore structure displayed by Bi_2WO_6 is consistent with the sheet morphology shown by SEM results.

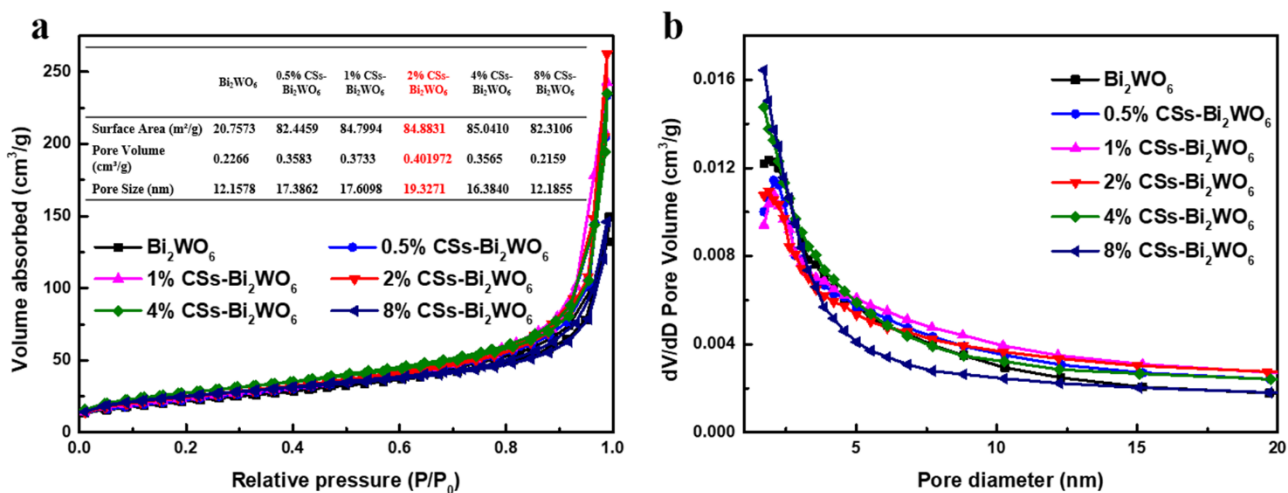


Fig. 3 N_2 adsorption-desorption isotherms (a), pore size distribution curves (the inset) of Bi_2WO_6 and CSs- Bi_2WO_6 (b)

3.2 Optical and electronic properties

It is well known that the utilization of visible light mainly depends on the band gap (E_g) and energy level of the semiconductor photocatalyst. The optical absorption abilities and bandgap of prepared samples were measured by DRS in Fig. 4.

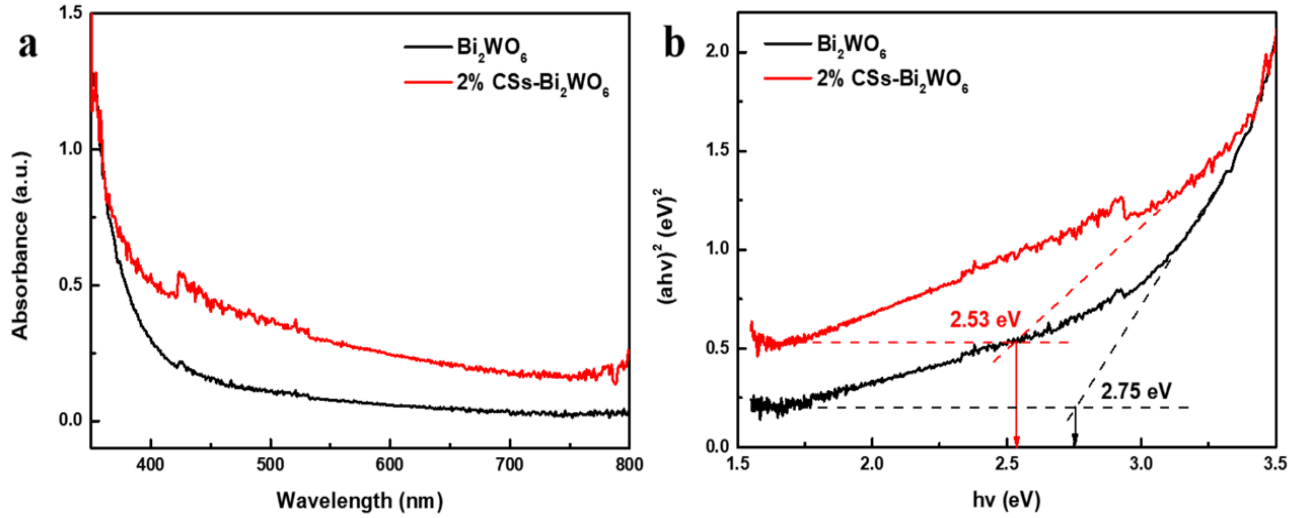


Fig. 4 UV-vis diffuse reflectance spectra of Bi_2WO_6 and 2% CSs- Bi_2WO_6 (a), plot of Kubelka - Munk transformation of Bi_2WO_6 and 2% CSs- Bi_2WO_6 (b)

Fig. 4a shows the comparison of UV-VIS DRS optical absorption characteristics between pure Bi_2WO_6 and 2% CSs- Bi_2WO_6 . It can be observed that the optical absorption capacity of 2% CSs- Bi_2WO_6 at 300-800 nm wavelength is higher than that of Bi_2WO_6 . In addition, after the introduction of CSs, the light absorption capacity of the sample has undergone a significant redshift. It shows that the composite photocatalyst has higher light utilization efficiency, promotes the transfer of charge, and improves photocatalytic performance. The band gaps energies (E_g) were calculated as the following formula [41]:

$$ahv = A(hv - E_g)^{\frac{n}{2}} \quad (1)$$

where A represents a constant, and α , ν , and E_g represent the adsorption coefficient, optical frequency, and bandgap, respectively [56]. The electronic transition type of the semiconductor determines the value of n [57]. Referring to previous studies, Bi₂WO₆ is an indirect bandgap semiconductor with an N value of 4 [58].

In Fig. 4b, the band gap of the pure Bi₂WO₆ was estimated to be 2.75 eV, which was consistent with the reported experimental values [59]. The band gap of the 2% CSs-Bi₂WO₆ sample was about 2.53 eV, which was lower than that of Bi₂WO₆.

Photoluminescence (PL) spectra is considered to be an important experiment to discuss the efficiency of e⁻ and h⁺ pair separation. Fig. 5a showed the strong emission peaks of the samples at 425 nm under excitation at 378 nm. In general, the emission intensity of CSs-Bi₂WO₆ was lower than that of pure Bi₂WO₆, and the 2% CSs-Bi₂WO₆ showed the lowest emission intensity, which proved its better photocatalytic activity. This trend suggested that the separation efficiency of photogenerated e⁻ and h⁺ can be effectively improved by introducing CSs, which promotes molecular diffusion and transfer.

In Fig. 5b, the flat-band (C_{FB}) potential of the composite photocatalyst is derived from the X-intercept of the linear region. And the obtained results can be further transformed into NHE potential [29, 60, 61]. The straight upward curves demonstrated that Bi₂WO₆ was an n-type semiconductor. The C_{FB} potentials of both the Bi₂WO₆ and 2% CSs-Bi₂WO₆ composites was -0.55 V vs. Ag/AgCl (-0.35 eV vs. NHE). The E_{CB} for both the Bi₂WO₆ and 2% CSs-Bi₂WO₆ Schottky contacts was approximately -0.45 eV. Combined with the E_g values obtained from Tauc plots in Fig. 4b, the valence band potentials (VB) of the 2% CSs-Bi₂WO₆ sample was calculated

to be 2.08 eV [62].

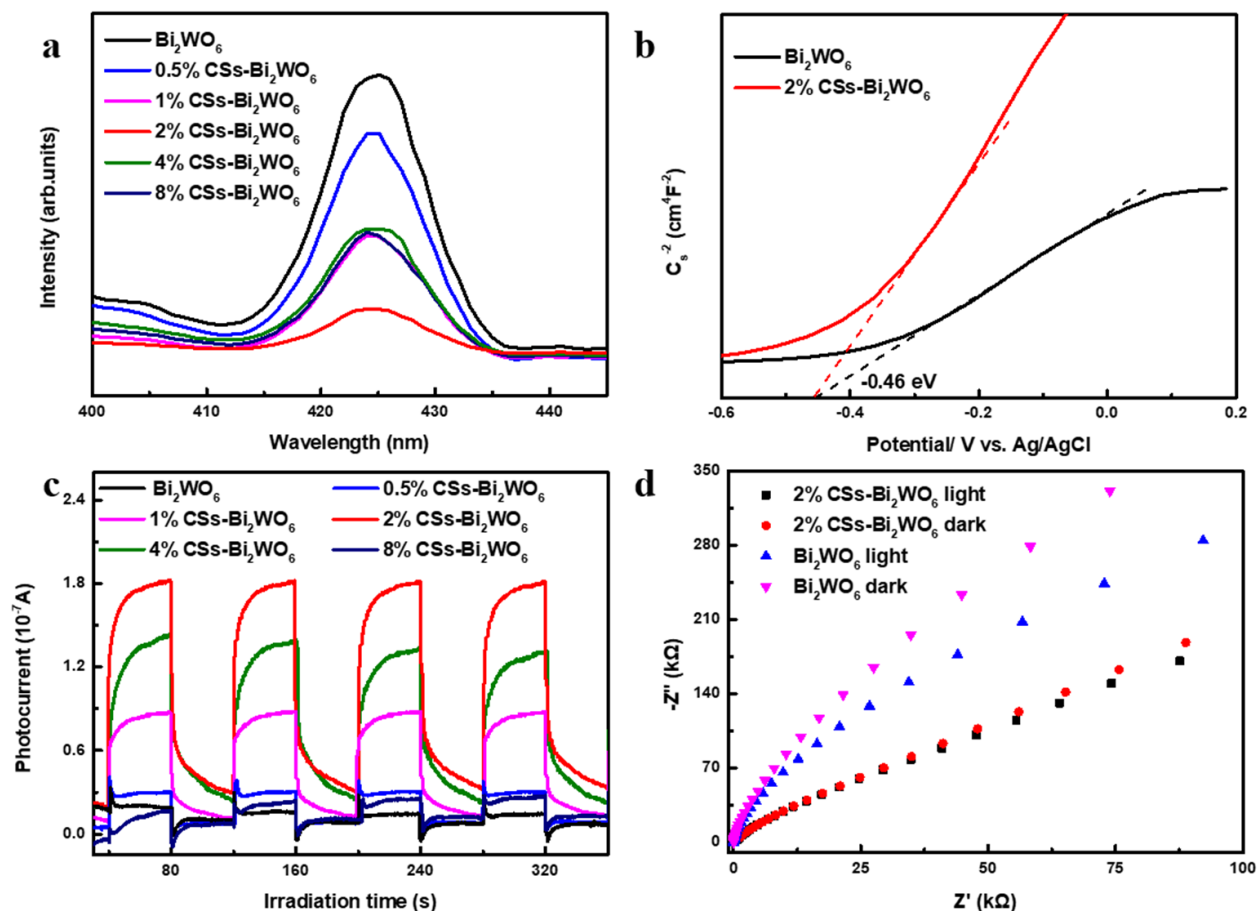


Fig. 5 PL spectra (a), Mott-Schottky curve of Bi_2WO_6 and 2% $\text{CSs-Bi}_2\text{WO}_6$ (b), transient photocurrent response of $\text{CSs-Bi}_2\text{WO}_6$ (c), electrochemical impedance spectroscopy (EIS) measurements of Bi_2WO_6 and 2% $\text{CSs-Bi}_2\text{WO}_6$ (d)

The photocurrent responses of the pure Bi_2WO_6 and 2% $\text{CSs-Bi}_2\text{WO}_6$ were tested and the results are displayed in Fig. 5c. Obviously, both the photoelectrodes of all samples show stable photocurrent responses over several switching cycles. All samples immediately produce a photocurrent when the electrode is momentarily exposed to visible light. On account of the higher recombination rate of photogenerated e^- and h^+ in the Bi_2WO_6 crystal, it can be found that Bi_2WO_6 had lower photocurrent responses. The photocurrent response of the composite photocatalyst 2% $\text{CSs-Bi}_2\text{WO}_6$ was about 9 times higher than pure Bi_2WO_6 , which effectively indicated more

efficient photo-induced charge separation and faster electron transport. Fig. 5d shows the EIS Nyquist plots for Bi_2WO_6 and 2% CSs- Bi_2WO_6 under different light conditions, respectively. The graph demonstrated that the arc radius of Bi_2WO_6 was larger than 2% CSs- Bi_2WO_6 , indicating that the introduction of CSs enhanced the charge migration of Bi_2WO_6 and reduces the reaction resistance at the semiconductor interface. Furthermore, the EIS semicircle radius of 2% CSs- Bi_2WO_6 under light is smaller than its under dark condition, which indicates that light can excite more charge carriers and enhance photocatalytic activity [63].

3.3 Photocatalytic tests

The photodegradation result of samples are shown in Fig. 6. TC was selected as the target pollutant to test its photocatalytic performance. Under visible light, 50 mg photocatalyst was added to 100 mL 50 mg / L TC solution for photocatalytic degradation. Fig. 6a is a diagram of the removal rate of TC by the catalyst. The composite photocatalyst reached adsorption-desorption equilibrium within 40 minutes of the dark reaction (adsorption kinetics data in Fig. S5). The degradation rate of TC by 2% CSs-Bi₂WO₆ was 84.6%, which is nearly 25% higher than pure Bi₂WO₆. This was because 2% CSs-Bi₂WO₆ had a large specific surface area, especially the folded structure of CSs, which effectively increased the adsorption of TC by the catalyst and promoted photoreaction. Notably, we found that the degradation effect of 0.5% CSs-Bi₂WO₆ was slightly higher than that of 1% CSs-Bi₂WO₆. In order to further explore its regularity, we added the photocatalytic degradation data of TC by 0.2% CSs-Bi₂WO₆ and 0.8% CSs-Bi₂WO₆ in the supporting information (Fig. S6) [64, 65]. However, even with the addition of a trace amount of CSs, the photocatalytic performance of the composite photocatalyst is still higher than that of pure BW, which indicates that CSs can effectively enhance the utilization of visible light and form a strong interfacial electronic effect with semiconductor and then improve the photocatalytic efficiency. Compared with the work reported in the literature on the degradation of organic pollutants by carbon materials in Table S2.

Fig. 6b shows the quasi-first-order degradation kinetics of the catalyst composite with a linear relationship between irradiation time and $\ln(C_0/C_t)$. The degradation rate constant was worked

from the slope of the kinetic curve. The rate constants for Bi_2WO_6 , 0.5% CSs- Bi_2WO_6 , 1% CSs- Bi_2WO_6 , 2% CSs- Bi_2WO_6 , 4% CSs- Bi_2WO_6 , and the 8% CSs- Bi_2WO_6 were 0.01502 min^{-1} , 0.00257 min^{-1} , 0.02141 min^{-1} , 0.03929 min^{-1} , 0.02951 min^{-1} and 0.0703 min^{-1} , respectively. In particular, 2% CSs- Bi_2WO_6 had the highest photocatalytic degradation rate, which should be put down to more efficient charge separation by adding CSs. The stability and reproducibility of photocatalysts are of great research value in practical applications. Fig. 6c shows the photocatalytic cycling test plots of the prepared catalyst samples. After the 5th cycle, the final degradation rate was about 80.5%, which displayed better photocatalytic stability of 2% CSs- Bi_2WO_6 .

We used different capture scavengers under visible light to explore the main active substances. In the present study: dimethyl sulfoxide (DMSO), ammonium oxalate (AMO), 1,4-benzoquinone (BQ), and isopropyl alcohol (IPA) were used as electron (e^-), hole (h^+), superoxide radical ($\cdot\text{O}_2^-$), and hydroxyl radical ($\cdot\text{OH}^-$) scavengers, respectively [66]. In Fig. 6d. the presence of BQ and AMO significantly inhibited the photodegradation of TC, indicating that $\cdot\text{O}_2^-$ was the main active species. Photodegradation was also somewhat inhibited when AMO was added into the system, indicating that the h^+ was more active in the composite photocatalyst. In addition, the addition of IPA and DMSO had little effect on the photocatalytic performance. In short, the order of action of the active species in the 2% CSs- Bi_2WO_6 photocatalytic degradation TC was $\cdot\text{O}_2^- > h^+ > e^- > \cdot\text{OH}^-$

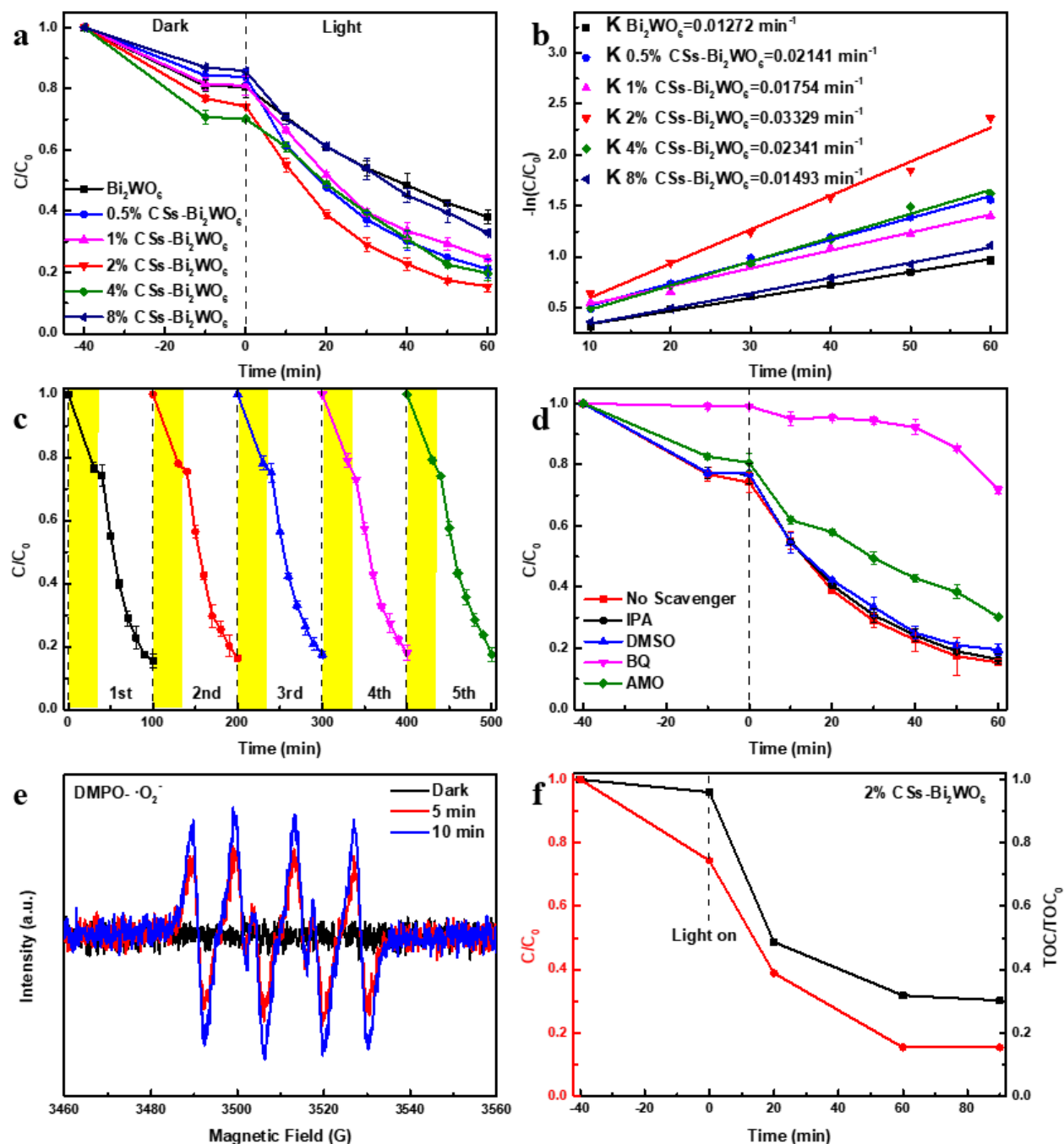


Fig. 6 Variation of TC concentration with irradiation time under light irradiation. (The experiment was repeated three times) (a), first-order kinetic curves of photocatalytic TC degradation in the as-synthesized samples (b), reusability of 2% CSs-Bi₂WO₆ in five runs for TC (c), mapping of active species captured in the TC photodegradation system on 2% CSs-Bi₂WO₆ under visible light (d), ESR spectrum of DMPO- $\cdot\text{O}_2^-$ (e), removal of TOC as a function of time for TC degradation using as-prepared 2% CSs-Bi₂WO₆ (f)

In Fig. 6e, a further identification test of the free radical O_2^- was carried out using electron

spin resonance (ESR). No ESR signal was observed in the dark condition. When 2% CSs-Bi₂WO₆ and DMPO were mixed under light for 5 and 10 minutes, a set of characteristic peaks attributed to ·O₂⁻ was found. This indicates that O₂⁻ was produced under light conditions in the catalytic system. The signal intensity of ·O₂⁻ increased with the increase of irradiation time. Relevant studies have shown that 2% CSs-Bi₂WO₆ photocatalytic TC not only has a higher degradation rate, but also a higher degree of organic matter mineralization [9, 67, 68]. Therefore, we studied the removal efficiency of total organic carbon (TOC), and the results are shown in Fig. 6f. It seems that in the 90 min degradation process, the reduction curve of TOC is mainly based on the degradation curve, and the degradation rate is 68.17%. TOC ratio was slightly higher than residual antibiotic concentration ratio, indicating that some intermediates were not completely degraded or degraded for a long time.

3.4 Photocatalytic mechanism

The intermediates of 2% CSs-Bi₂WO₆ photodegradation of TC were identified by LC-MS technology, and the degradation pathway of TC was further described. 12 intermediates with m/z values of 481, 475, 459, 445, 415, 388, 344, 318, 300, 274, 250, 246, 242, and 165 were generated under visible light irradiation. According to Fig. 6d, ·O₂⁻ was the main active substance in the degradation process. Therefore, the photodegradation pathway of TC can be proposed (Fig. 7 and Fig. S7) [69, 70].

After visible light irradiation, TC was invaded from three possible sites. Pathway 1: The main reaction pathway of TC degradation is the reaction of superoxide radical attacking phenol group. Under light conditions, it was further oxidized to form a macromolecular intermediate with m/z = 475. Then, the product with m/z = 475 was converted to the product with m/z = 459 by attacking the ketone group and changing the hydroxyl group [71]. Finally, the unstable intermediate cleaved due to the loss of the hydroxyl group, resulting in the formation of small molecules with m/z of 344, 300 and 242, respectively. They are eventually mineralized into H₂O and CO₂. Pathway 2: The formation of m/z = 481 is due to the attack of the double bond of TC, which further introduces hydroxyl and ketone groups [72]. In the next period, the product of m/z = 246 and 165 appears due to the opening of the benzene ring by h⁺ attack. Eventually mineralized into small molecules [73]. Pathway 3: the product of m/z = 338 was attributed to the loss of the N-methyl group. The product with m/z = 318 is formed due to further cleavage of the C-ring and loss of the hydroxyl group. Furthermore, the small

molecule with $m/z = 318$ was transformed into a product with $m/z = 274$ by removing the carboxyl group. Finally, after different process of detachment of hydroxyl, and aldehyde groups followed by decarbonization and dihydroxylation [74]. With increasing reaction time, oxidative decomposition and ring-opening reactions further occur, and the above intermediate products are finally decomposed into H_2O , CO_2 and NH_4^+ , etc.

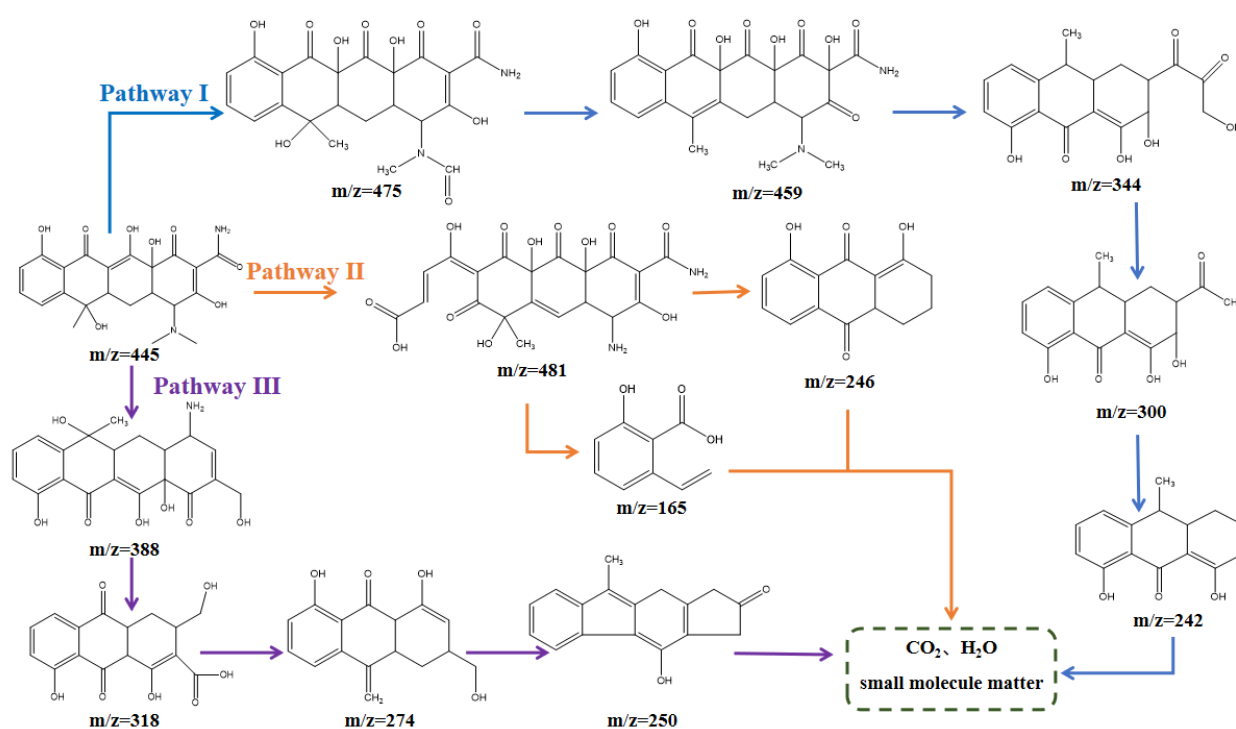
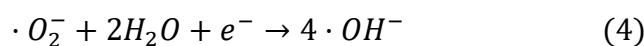


Fig. 7 Degradation pathway of TC over 2% CSs-Bi₂WO₆

According to the above experiments, Fig. 8 shows the mechanism of photocatalytic degradation of TC by 2% CSs-Bi₂WO₆ under visible light irradiation. The CB of 2% CSs-Bi₂WO₆ was - 0.45 eV, which was more negative than the redox potential ($E_{O_2/O_2^-} = - 0.33$ eV). Thus, the main reason for TC degradation was that the photogenerated electrons were transferred to O₂ and further converted to $\cdot O_2^-$. In

addition, combined with the E_g energy of 2% CSs-Bi₂WO₆, the VB potential of 2% CSs-Bi₂WO₆ can be deduced as + 2.08 eV according to the equation ($E_{CB} = E_{VB} - E_g$) [75]. Specific data are described in Fig. 4. The VB level of 2% CSs-Bi₂WO₆ was lower than $E_{\cdot OH/OH^-} = + 2.31$ eV. Therefore, $\cdot OH^-$ did not play a major role in the photocatalytic reaction. Under visible light irradiation, the semiconductor photocatalyst generates electron-hole pairs. The photogenerated electrons reacted with O₂ (from the air) on the photocatalyst surface to form the $\cdot O_2^-$. TC is eventually mineralized into small molecule compounds, such as water and carbon dioxide [38, 76]. To sum up, the 2% CSs-Bi₂WO₆ photocatalyst has higher electron-hole separation efficiency than the bare Bi₂WO₆ photocatalyst. Further, the photodegradation reaction process of TC has been proposed as Equations (2-6):



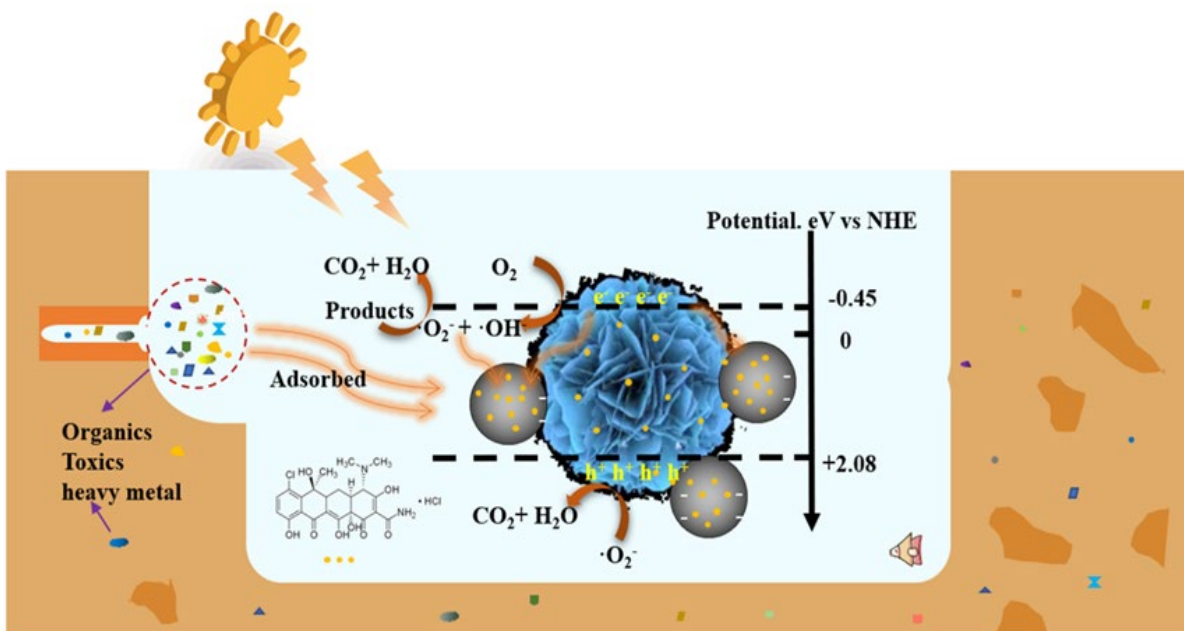


Fig. 8 Possible mechanism of TC on the surface of 2% CSs-Bi₂WO₆ composite

During the dark reaction, TC was adsorbed on the surface of CSs due to irregular folds on the surface and strong adsorption. It facilitated the transfer of pollutants from the environment to the surface of the catalyst, forming a high concentration TC environment on the surface. And finally adsorption - dissolution equilibrium was achieved. In addition, CSs are more efficient at harvesting light by multiple scattering and utilizing photons. The composite can effectively separate the e^- / h^+ pairs when photogenerated electrons in bismuth tungstate migrate to the CSs, thus improving the photocatalytic performance.

4 Conclusion

In summary, the composite photocatalyst of CSs-Bi₂WO₆ was synthesized by a simple hydrothermal method. The experimental results showed that the composite showed good photocatalytic performance (84.6%) and stability for tetracycline degradation under the optimal CSs loading amount (2 wt%). The degradation kinetics of TC in CSs modified Bi₂WO₆ was 2.6 times that of pure Bi₂WO₆. This may be because CSs can enhance the absorption of visible light by the composite catalyst and effectively enhance the separation efficiency of e⁻/h⁺. It is worth noting that the TOC estimation of the post-degradation reaction medium corresponded to 68.2% mineralization. Based on the capture experiment and ESR measurement results, the free radical ·O₂⁻ plays a leading role in the photocatalytic reaction. Further, the photocatalytic reaction mechanism and degradation pathway of 2% CSs-Bi₂WO₆ were revealed in detail by using LC-MS determined reaction intermediates. This study provides a new idea for photocatalytic degradation of organic pollutants through the synergistic action of carbon and semiconductor materials.

Acknowledgements

We thank Dr. Zhanhua Huang for the guidance and help in the experiment and writing of the paper. This work was supported by the National Natural Science Foundation of China (No. 32071713), the Outstanding Youth Foundation Project of Heilongjiang Province (No. JQ2019C001), and Northeast Forestry University College Student Innovation Training Program Funding Project (No. CL202210225471).

Author Contributions Statement

Zhanhua Huang: conceptualization, methodology, writing - review and editing, Funding acquisition. Xiaona Jiang, Xinrui Zhang, and Houjuan Qi wrote the main manuscript text. Shuai Chen and Lanni Qu prepared figures. All authors reviewed the manuscript.

Declaration of Competing Interest

There are no conflicts to declare.

Funding

The National Natural Science Foundation of China (No. 32071713);

The Outstanding Youth Foundation Project of Heilongjiang Province (No. JQ2019C001);

The Northeast Forestry University College Student Innovation Training Program Funding Project (No. CL202210225471).

References:

- [1] Nan JJ, Guo SJ, Alhashmialameer D, He QM; Meng YN, Ge RX, El-Bahy SM, Naik, N, Murugadoss V, Huang MN, Xu BB, Shao Q, Guo ZH (2022) Hydrothermal Microwave Synthesis of $\text{Co}_3\text{O}_4/\text{In}_2\text{O}_3$ Nanostructures for Photoelectrocatalytic Reduction of Cr (VI). *ACS Appl Nano Mater* 5:8755-8766.
<https://doi.org/10.1021/acsanm.2c00107>
- [2] Sun JF, Mu Q, Kimura H, Murugadoss V, He MX, Du W, Hou CX (2022) Oxidative degradation of phenols and substituted phenols in the water and atmosphere: a review. *Adv Compos Hybrid Ma* 5(2):627-640. <https://doi.org/10.1007/s42114-022-00435-0>
- [3] Hong JM, Kang L, Shi XF, Wei RB, Mai XM, Pan D, Naik N, Guo ZH (2022) Highly efficient removal of trace lead (II) from wastewater by 1,4-dicarboxybenzene modified Fe/Co metal organic nanosheets. *J Mater Sci Technol* 98:212-218.
<https://doi.org/10.1016/j.jmst.2021.05.021>
- [4] Wu QZ, Gao LS, Huang MN, Mersal GAM, Ibrahim MM, El-Bahy ZM, Shi XF, Jiang QL (2022) Aminated lignin by ultrasonic method with enhanced arsenic (V) adsorption from polluted water. *Adv Compos Hybrid Ma* 5:1044-1053.
<https://doi.org/10.1007/s42114-022-00492-5>
- [5] Li ZH, Xie WH, Yao FC, Du A, Wang QY, Guo ZH, Gu HB (2022) Comprehensive electrocatalytic degradation of tetracycline in wastewater by electrospun perovskite manganite nanoparticles supported on carbon nanofibers. *Adv Compos Hybrid Ma* 5:2092-2105. <https://doi.org/10.1007/s42114-022-00550-y>
- [6] Li ZT, Xu XT, Sheng XR, Lin P, Tang J, Pan LK, Kaneti YV, Yang T, Yamauchi Y (2021) Solar-powered sustainable water production: state-of-the-art technologies for sunlight energy-water nexus. *ACS Nano* 15:12535-12566.
<https://doi.org/10.1021/acsnano.1c01590>
- [7] Wang ZZ, Jiang LS, Wang K, Li Y, Zhang GK (2021) Novel AgI/BiSbO₄ heterojunction for efficient photocatalytic degradation of organic pollutants under visible light: Interfacial electron transfer pathway, DFT calculation and degradation mechanism study. *J Hazard Mater* 410:124948.
<https://doi.org/10.1016/j.jhazmat.2020.124948>
- [8] Adhikari S, Lee HH, Kim D-H (2020) Efficient visible-light induced electron-transfer in z-scheme $\text{MoO}_3/\text{Ag}/\text{C}_3\text{N}_4$ for excellent photocatalytic removal of antibiotics of both ofloxacin and tetracycline. *Chem Eng J* 391:123504.
<https://doi.org/10.1016/j.cej.2019.123504>
- [9] Jourshabani M, Asrami MR, Lee BK (2022) An efficient and unique route for the fabrication of highly condensed oxygen-doped carbon nitride for the photodegradation of synchronous pollutants and H_2O_2 production under ambient conditions. *Appl Catal B-Environ* 302:120839. <https://doi.org/10.1016/j.apcatb.2021.120839>
- [10] Alatalo SM, Daneshvar E, Kinnunen N, Mesceriakovas A, Thangaraj SK, Janis J, Tsang DCW, Bhatnagar A, Lahde A (2019) Mechanistic insight into efficient removal of tetracycline from water by Fe/graphene. *Chem Eng J* 373:821-830.
<https://doi.org/10.1016/j.cej.2019.05.118>

- [11] Malik AH, Iyer PK (2017) Conjugated polyelectrolyte based sensitive detection and removal of antibiotics tetracycline from water. *ACS Appl Mater Inter* 9:4433-4439. <https://doi.org/10.1021/acsami.6b13949>
- [12] Chankhanittha T, Somaudon V, Photiwat T, Hemavibool K, Nanan S (2021) Preparation, characterization, and photocatalytic study of solvothermally grown CTAB-capped Bi_2WO_6 photocatalyst toward photodegradation of Rhodamine B dye. *Opt Mater* 117:111183. <https://doi.org/10.1016/j.optmat.2021.111183>
- [13] Rambabu K, Bharath G, Banat F, Show PL (2020) Green synthesis of zinc oxide nanoparticles using Phoenix dactylifera waste as bioreductant for effective dye degradation and antibacterial performance in wastewater treatment. *J Hazard Mater* 402:123560. <https://doi.org/10.1016/j.hazmat.2020.123560>
- [14] Wang YF, Zhang HT, Xie J, Liu YX, Wang SL, Zhao QF (2020) Three-dimensional mesoporous carbon nanospheres as carriers for chemo-photothermal therapy compared with two-dimensional graphene oxide nanosheets. *Colloid Surface A* 590:124498. <https://doi.org/10.1016/j.colsurfa.2020.124498>
- [15] Hu T, Li YM, Gao W, Wang XF, Tian Y (2019) Engineering of rich nitrogen-doped and magnetic mesoporous carbon nanospheres with predictable size uniformity for acid dye molecules adsorption. *Micropor Mesopor Mat* 279:234-244. <https://doi.org/10.1016/j.micromeso.2018.12.034>
- [16] Zou ZM, Yang XY, Zhang P, Zhang YM, Yan XX, Zhou RM, Liu D, Xu L, Gui JZ (2019) Trace carbon-hybridized ZnS/ZnO hollow nanospheres with multi-enhanced visible-light photocatalytic performance. *J Alloy Compd* 775:481-489. <https://doi.org/10.1016/j.jallcom.2018.10.116>
- [17] Chen YY, Wang Y, Li Z, Wang DD, Yuan H, Zhang HZ, Tan YQ (2021) A flame retarded polymer-based composite solid electrolyte improved by natural polysaccharides. *Compos Commun* 26:100774. <https://doi.org/10.1016/j.coco.2021.100774>
- [18] Liu W, He TP, Wang YH, Ning G, Xu ZG, Chen XY, Hu XJ, Wu YH, Zhao YL (2020) Synergistic adsorption-photocatalytic degradation effect and norfloxacin mechanism of ZnO/ZnS@BC under UV-light irradiation. *Sci Rep-UK* 10:1-12. <https://doi.org/10.1038/s41598-020-68517-x>
- [19] Li N, Fan GD, Fan MM, Wu F, Zhang GX, Fan D (2021) All-solid-state Z-scheme $\text{Ag}_3\text{PO}_4/\text{CSs}/\text{AgBr}$ heterostructures for efficient visible-light photocatalysis and the photocatalytic mechanism. *Dalton T* 50:15602-15611. <https://doi.org/10.1039/d1dt02937a>
- [20] Chen Z, Li XM, Xu QX, Tao Z, Yao FB, Huang XD, Wu Y, Wang DB, Jiang PH, Yang Q (2020) Three-dimensional network space $\text{Ag}_3\text{PO}_4/\text{NP-CQDs}/\text{rGH}$ for enhanced organic pollutant photodegradation: Synergetic photocatalysis activity/stability and effect of real water quality parameters. *Chem Eng J* 390:124454. <https://doi.org/10.1016/j.cej.2020.124454>
- [21] Xu ZN, Jiang JX, Zhang QQ, Chen GB, Zhou LM, Li L (2020) 3D graphene aerogel composite of 1D-2D Nb_2O_5 -g- C_3N_4 heterojunction with excellent adsorption and visible-light photocatalytic performance. *J Colloid Interf Sci* 563:131-138. <https://doi.org/10.1016/j.jcis.2019.12.002>

- [22] Rafiq A, Ikram M, Ali S, Niaz F, Khan M, Khan Q, Maqbool M (2021) Photocatalytic degradation of dyes using semiconductor photocatalysts to clean industrial water pollution. *J Ind Eng Chem* 97:111-128.
<https://doi.org/10.1016/j.jiec.2021.02.017>
- [23] Sharma S, Dutta V, Singh P, Raizada P, Rahmani-Sani A, Hosseini-Bandegharai A, Thakur VK (2019) Carbon quantum dot supported semiconductor photocatalysts for efficient degradation of organic pollutants in water: a review. *J Clean Prod* 228:755-769. <https://doi.org/10.1016/j.jclepro.2019.04.292>
- [24] Chai FJ, Meng FL, Liu S, Zhang Y, Yang T, Jia YF, Li SJ, Yuan XH (2022) A novel Bi₂O₃ modified C-doped hollow TiO₂ sphere based on glucose-derived carbon sphere with enhanced visible light photocatalytic activity. *J Inorg Organomet* 32:2298-2308.
<https://doi.org/10.1007/s10904-022-02291-3>
- [25] Wang XT, Zhou JQ, Zhao SZ, Chen X, Yu Y (2018) Synergistic effect of adsorption and visible-light photocatalysis for organic pollutant removal over BiVO₄/carbon sphere nanocomposites. *Appl Surf Sci* 453:394-404.
<https://doi.org/10.1016/j.apsusc.2018.05.073>
- [26] Zhang YF, Shao Q, Murugadoss V, Maganti S, Naik N, Algadi, H, Huang MA (2022) Influence of mass ratio and calcination temperature on physical and photoelectrochemical properties of ZnFe-layered double oxide/cobalt oxide heterojunction semiconductor for dye degradation applications. *Particuology* 74:141-155. <https://doi.org/10.1016/j.partic.2022.05.010>
- [27] Adhikari S, Kim DH (2018) Synthesis of Bi₂S₃/Bi₂WO₆ hierarchical microstructures for enhanced visible light driven photocatalytic degradation and photoelectrochemical sensing of ofloxacin. *Chem Eng J* 354:692-705.
<https://doi.org/10.1016/j.cej.2018.08.087>
- [28] Lu T, Gao Y, Yang Y, Ming HB, Huang ZC, Liu GD, Zheng DD, Zhang JS, Hou YD (2021) Efficient degradation of tetracycline hydrochloride by photocatalytic ozonation over Bi₂WO₆. *Chemosphere* 283:131256.
<https://doi.org/10.1016/j.chemosphere.2021.131256>
- [29] Hao XQ, Wang YC, Zhou J, Cui ZW, Wang Y, Zou ZG (2018) Zinc vacancy-promoted photocatalytic activity and photostability of ZnS for efficient visible-light-driven hydrogen evolution. *Appl Catal B-Environ* 221:302-311.
<https://doi.org/10.1016/j.apcatb.2017.09.006>
- [30] Hu JD, Chen DY, Mo Z, Li NJ, Xu QF, Li H, He JH, Xu H, Lu JM (2019) Z-Scheme 2D/2D heterojunction of black phosphorus/monolayer Bi₂WO₆ nanosheets with enhanced photocatalytic activities. *Angew Chem Int Edit* 58:2073-2077.
<https://doi.org/10.1002/anie.201813417>
- [31] Lv N, Li YY, Huang ZL, Li T, Ye SY, Dionysiou DD, Song XL (2019) Synthesis of GO/TiO₂/Bi₂WO₆ nanocomposites with enhanced visible light photocatalytic degradation of ethylene. *Appl Catal B-Environ* 246:303-311.
<https://doi.org/10.1016/j.apcatb.2019.01.068>
- [32] Li PB, Zhao XQ, Dai JX, Han YF, Jiang JH, Zhang Y (2022) Preparation of large-faced flower-like Bi₂WO₆ using carbon as a template to enhanced photocatalytic activity under visible light. *J Phys Chem Solids* 171:110968.

- <https://doi.org/10.1016/j.jpccs.2022.110968>
- [33] Cai MJ, Wang CC, Liu YP, Yan RY, Li SJ (2022) Boosted photocatalytic antibiotic degradation performance of Cd_{0.5}Zn_{0.5}S/carbon dots/Bi₂WO₆ S-scheme heterojunction with carbon dots as the electron bridge. *Sep Purif Technol* 300:121892. <https://doi.org/10.1016/j.seppur.2022.121892>
- [34] Yan FY, Wang Y, Yi CH, Xu JX, Wang BW, Ma R, Xu M (2022) Construction of carbon dots modified Cl-doped Bi₂WO₆ hollow microspheres for boosting photocatalytic degradation of tetracycline under visible light irradiation. *Ceram Int* 2. <https://doi.org/10.1016/j.ceramint.2022.05.258>
- [35] Lei SY, Qin C, Tang XL, Zhong JB, Li JZ, Chen J (2020) Spiral carbon fibers modified Bi₂WO₆ with enhanced photocatalytic activity. *J Phys Chem Solids* 141:109430. <https://doi.org/10.1016/j.jpccs.2020.109430>
- [36] Wang JW, Zhang WK, Zhang XB, Wang FM, Yang YQ, Lv GJ (2020) Enhanced photocatalytic ability and easy retrievable photocatalysts of Bi₂WO₆ quantum dots decorated magnetic carbon nano-onions. *J Alloy Compd* 826:154217. <https://doi.org/10.1016/j.jallcom.2020.154217>
- [37] Shad NA, Sajid MM, Afzal AM, Amin N, Javed Y, Hassan S, Imran Z, Razaq A, Yousaf MI, Munawar A, Sharma SK (2021) Facile synthesis of Bi₂WO₆/rGO nanocomposites for photocatalytic and solar cell applications. *Ceram Int* 47:16101-16110. <https://doi.org/10.1016/j.ceramint.2021.02.185>
- [38] Kadeer K, Tursun Y, Dilinuer T, Okitsu K, Abulizi A (2018) Sonochemical preparation and photocatalytic properties of CdS QDs/Bi₂WO₆ 3D heterojunction. *Ceram Int* 44:13797-13805. <https://doi.org/10.1016/j.ceramint.2018.04.223>
- [39] Hua CH, Wang JW, Dong XL, Wang Y, Zheng N, Xue M, Zhang XX (2020) In situ plasmonic Bi grown on I⁻ doped Bi₂WO₆ for enhanced visible-light-driven photocatalysis to mineralize diverse refractory organic pollutants. *Sep Purif Technol* 250:117119. <https://doi.org/10.1016/j.seppur.2020.117119>
- [40] Wu B, Liu D, Mubeen S, Chuong TT, Moskovits M, Stucky GD (2016) Anisotropic growth of TiO₂ onto gold nanorods for plasmon-enhanced hydrogen production from water reduction. *J Am Chem Soc* 138:1114-1117. <https://doi.org/10.1021/jacs.5b11341>
- [41] Wu H, Wu XL, Mine S, Matsuoka M, Chu YH, Wang ZM (2020) Crafting carbon sphere-titania core-shell interfacial structure to achieve enhanced visible light photocatalysis. *Appl Surf Sci* 534:147566. <https://doi.org/10.1016/j.apsusc.2020.147566>
- [42] Chen P, Chen L, Zeng Y, Ding F, Jiang X, Liu N, Au CT, Yin SF (2018) Three-dimension hierarchical heterostructure of CdWO₄ microrods decorated with Bi₂WO₆ nanoplates for high-selectivity photocatalytic benzene hydroxylation to phenol. *Appl Catal B-Environ* 234:311-317. <https://doi.org/10.1016/j.apcatb.2018.04.028>
- [43] Kumar P, Vahidzadeh E, Thakur UK, Kar P, Alam KM, Goswami A, Mahdi N, Cui K, Bernard GM, Michaelis VK, Shankar K (2019) C₃N₅: a low bandgap semiconductor containing an azo-linked carbon nitride framework for photocatalytic, photovoltaic and adsorbent applications. *J Am Chem Soc* 141:5415-5436. <https://doi.org/10.1021/jacs.9b00144>

- [44] Sharma V, Kumar A, Kumar A, Krishnan V (2022) Enhanced photocatalytic activity of two-dimensional ternary nanocomposites of ZnO-Bi₂WO₆-Ti₃C₂ MXene under natural sunlight irradiation. *Chemosphere* 287:132119. <https://doi.org/10.1016/j.chemosphere.2021.132119>
- [45] Zhu BK, Song DB, Jia TB, Sun WY, Wang DG, Wang LH, Guo J, Jin LH, Zhang L, Tao HC (2021) Effective visible light-driven photocatalytic degradation of ciprofloxacin over flower-like Fe₃O₄/Bi₂WO₆ composites. *ACS omega* 6:1647-1656. <https://doi.org/10.1021/acsomega.0c05616>
- [46] Gong JW, Guo YZ, Lu J, Cheng Y, Wang HS (2022) TEMPO oxidized nanofiber carbon quantum dots/TiO₂ composites with enhanced photocatalytic activity for degradation of methylene blue. *Chem Phys Lett* 788:139297. <https://doi.org/10.1016/j.cplett.2021.139297>
- [47] Manchala S, Gandamalla A, Vempuluru NR, Venkatakrishnan SM, Shanker V (2021) High potential and robust ternary LaFeO₃/CdS/carbon quantum dots nanocomposite for photocatalytic H₂ evolution under sunlight illumination. *JJ Colloid Interf Sci* 583:255-266. <https://doi.org/10.1016/j.jcis.2020.08.125>
- [48] Wang YP, Sun XF, Xian T, Liu GR, Yang H (2021) Photocatalytic purification of simulated dye wastewater in different pH environments by using BaTiO₃/Bi₂WO₆ heterojunction photocatalysts. *Opt Mater* 113:110853. <https://doi.org/doi:10.1016/j.optmat.2021.110853>
- [49] Li K, Xie X, Zhang WD (2016) Photocatalysts based on g-C₃N₄-encapsulating carbon spheres with high visible light activity for photocatalytic hydrogen evolution. *Carbon* 110:356-366. <https://doi.org/10.1016/j.carbon.2016.09.039>
- [50] Dehkordi AB, Badiie A (2021) Insight into the activity of TiO₂@nitrogen-doped hollow carbon spheres supported on g-C₃N₄ for robust photocatalytic performance. *Chemosphere* 288:132392. <https://doi.org/10.1016/j.chemosphere.2021.132392>
- [51] Chen YX, Ji XB, Vadivel S, Paul B (2018) Anchoring carbon spheres on BiOBr/g-C₃N₄ matrix for high-performance visible light photocatalysis. *Ceram Int* 44:23320-23323. <https://doi.org/10.1016/j.ceramint.2018.09.070>
- [52] Yang WY, Peng DN, Kimura H, Zhang XY, Sun XQ, Pashameah RA, Alzahrani E, Wang B, Guo ZH, Du W, Hou C (2022) Honeycomb-like nitrogen-doped porous carbon decorated with Co₃O₄ nanoparticles for superior electrochemical performance pseudo-capacitive lithium storage and supercapacitors. *Adv Compos Hybrid Ma* 5:3146-3157. <https://doi.org/10.1007/s42114-022-00556-6>
- [53] Zhang YM, Liu LY, Zhao LL, Hou CX, Huang MN, Algadi H, Li DY, Xia Q, Wang J, Zhou ZR, Han X, Long YX, Li YB, Zhang ZD, Liu Y (2022) Sandwich-like CoMoP₂/MoP heterostructures coupling N, P co-doped carbon nanosheets as advanced anodes for high-performance lithium-ion batteries. *Adv Compos Hybrid Ma* 5:2601-2610. <https://doi.org/10.1007/s42114-022-00535-x>
- [54] He JY, Yu Q, Zhou YP, Wang YV, Long F (2020) Rare Earth Ion Yb³⁺ Doping of Bi₂WO₆ with Excellent Visible-light Photocatalytic Activity. *J Wuhan Univ Technol* 35:348-355. <https://doi.org/10.1007/s11595-020-2263-z>
- [55] Tang YD, Li T, Xiao WX, Huang ZT, Wen HC, Situ WB, Song XL (2023) Degradation mechanism and pathway of tetracycline in milk by heterojunction N-TiO₂-

- Bi₂WO₆ film under visible light. *Food Chem* 401:134082.
<https://doi.org/10.1016/j.foodchem.2022.134082>
- [56] Chen SQ, Li F, Li TH, Cao W (2019) Loading AgCl@ Ag on phosphotungstic acid modified macrocyclic coordination compound: Z-scheme photocatalyst for persistent pollutant degradation and hydrogen evolution. *J Colloid Interface Sci* 547:50-59.
<https://doi.org/10.1016/j.jcis.2019.03.092>
- [57] Wang WL, Zhao WL, Zhang HC, Dou XC, Shi HF (2020) 2D/2D step-scheme alpha-Fe₂O₃/Bi₂WO₆ photocatalyst with efficient charge transfer for enhanced photo-Fenton catalytic activity. *Chinese J Catal* 42:97-106. <https://doi.org/10.1063/1.323948>
- [58] Meng XC, Zhang ZS (2015) Synthesis, analysis, and testing of BiOBr-Bi₂WO₆ photocatalytic heterojunction semiconductors. *Int J Photoenergy* 4:1-12.
<https://doi.org/10.1155/2015/630476>
- [59] Qiang ZM, Liu XM, Li F, Li TH, Zhang M, Singh H, Huttula M, Cao W (2021) Iodine doped Z-scheme Bi₂O₂CO₃/Bi₂WO₆ photocatalysts: Facile synthesis, efficient visible light photocatalysis, and photocatalytic mechanism. *Chem Eng J* 403:126327.
<https://doi.org/10.1016/j.cej.2020.126327>
- [60] Giannakopoulou T, Papailias I, Todorova N, Boukos N, Liu Y, Yu J, Trapalis C (2016) Tailoring the energy band gap and edges' potentials of g-C₃N₄/TiO₂ composite photocatalysts for NO_x removal. *Chem Eng J* 310:571-580.
<https://doi.org/10.1016/j.cej.2015.12.102>
- [61] Zhang YL, Zhao YC, Xiong Z, Gao T, Gong BG, Liu PF, Liu J, Zhang JY (2020) Elemental mercury removal by I-doped Bi₂WO₆ with remarkable visible-light-driven photocatalytic oxidation. *Environmental Research* 282:119534.
<https://doi.org/10.1016/j.apcatb.2020.119534>
- [62] Zhang SJ, Huang WX, Fu XL, Chen GL, Meng SG, Chen SF (2018) Ultra-low content of Pt modified CdS nanorods: Preparation, characterization, and application for photocatalytic selective oxidation of aromatic alcohols and reduction of nitroarenes in one reaction system. *J Hazard Mater* 360:182-192.
<https://doi.org/10.1016/j.jhazmat.2018.07.108>
- [63] Zhang QZ, Deng JJ, Xu ZH, Chaker M, Ma DD (2017) High-efficiency broadband C₃N₄ photocatalysts: synergistic effects from upconversion and plasmons. *ACS Catal* 7:6225-6234. <https://doi.org/10.1021/acscatal.7b02013>
- [64] Cheng G, Xu FF, Xiong JY, Tian F, Ding J, Stadler FJ, Chen R (2016) Enhanced adsorption and photocatalysis capability of generally synthesized TiO₂-carbon materials hybrids. *Adv Powder Technol* 27:1949-1962.
<https://doi.org/10.1016/j.apt.2016.06.026>
- [65] Shi JH, Chen T, Guo CL, Liu ZC, Feng ST, Li YZ, Hu J (2019) The bifunctional composites of AC restrain the stack of g-C₃N₄ with the excellent adsorption-photocatalytic performance for the removal of RhB. *Colloids and Surfaces A: Physicochemical and Engineering Aspects* 580:123701.
<https://doi.org/10.1016/j.colsurfa.2019.123701>
- [66] Guan ZL, Li XM, Wu Y, Chen Z, Huang XD, Wang DB (2021) AgBr nanoparticles decorated 2D/2D GO/Bi₂WO₆ photocatalyst with enhanced photocatalytic performance for the removal of tetracycline hydrochloride. *Chem Eng J* 410:128283.

- <https://doi.org/10.1016/j.cej.2020.128283>
- [67] Jourshabani M, Yun SH, Asrami MR, Lee BK (2022) Superior photodegradation of organic compounds and H₂O₂ production over tungsten oxide/carbon nitride heterojunction with sizable heptazine units: Dual polycondensation and interface engineering. *Chem Eng J* 427:131710. <https://doi.org/10.1016/j.cej.2021.131710>
- [68] Jing C, Zhang YF, Zheng JJ, Ge SS, Lin J, Pan D, Naik N, Guo ZH (2022) In-situ constructing visible light CdS/Cd-MOF photocatalyst with enhanced photodegradation of methylene blue. *Particuology* 69:111-122. <https://doi.org/10.1016/j.partic.2021.11.013>
- [69] Lu Q, Dong CC, Wei F, Li JD, Wang Z, Mu W, Han XJ (2022) Rational fabrication of Bi₂WO₆ decorated TiO₂ nanotube arrays for photocatalytic degradation of organic pollutants. *Mater Res Bull* 145:111563. <https://doi.org/10.1016/j.materresbull.2021.111563>
- [70] Xu J, Zhu P, ElAzab IH, Xu BB, Guo ZH, Elnaggar AY, Mersal GAM, Liu XY, Zhi YF, Lin ZP, H. Algadi, S. Shan (2022) An efficient bifunctional Ni-Nb₂O₅ nanocatalysts for the hydrodeoxygenation of anisole. *Chinese J Chem Eng* 49:187-197. <https://doi.org/10.1016/j.cjche.2022.07.009>
- [71] Chen YX, Yin RL, Zeng LX, Guo WQ, Zhu MS (2021) Insight into the effects of hydroxyl groups on the rates and pathways of tetracycline antibiotics degradation in the carbon black activated peroxydisulfate oxidation process. *J Hazard Mater* 412:125256. <https://doi.org/10.1016/j.jhazmat.2021.125256>
- [72] Guan ZL, Li XM, Wu W, Chen Z, Huang XD, Wang DB, Yang Q, Liu JL, Tian SH, Chen XY, Zhao H (2021) AgBr nanoparticles decorated 2D/2D GO/Bi₂WO₆ photocatalyst with enhanced photocatalytic performance for the removal of tetracycline hydrochloride. *Chem Eng J* 410:128283. <https://doi.org/10.1016/j.cej.2020.128283>
- [73] Deng SY, Li ZZ, Zhao TS, Huang GC, Wang JC, Bi JH (2022) Direct Z-scheme covalent triazine-based framework/Bi₂WO₆ heterostructure for efficient photocatalytic degradation of tetracycline: Kinetics, mechanism and toxicity. *J Water Process Eng* 49:103021. <https://doi.org/10.1016/j.jwpe.2022.103021>
- [74] Kaur M, Mehta SK, Devi P, Kansal SK (2021) Bi₂WO₆/NH₂-MIL-88B(Fe) heterostructure: An efficient sunlight driven photocatalyst for the degradation of antibiotic tetracycline in aqueous medium. *Adv Powder Technol* 32:4788-4804. <https://doi.org/10.1016/j.apt.2021.10.025>
- [75] Gao X, Niu J, Wang YF, Ji Y, Zhang YL (2021) Solar photocatalytic abatement of tetracycline over phosphate oxoanion decorated Bi₂WO₆/polyimide composites. *J Hazard Mater* 403:123860. <https://doi.org/10.1016/j.jhazmat.2020.123860>
- [76] Sun J, Shen CH, Guo J, Guo H, Yin YF, Xu XJ, Fei ZH, Liu ZT, Wen XJ (2021) Highly efficient activation of peroxymonosulfate by Co₃O₄/Bi₂WO₆ p-n heterojunction composites for the degradation of ciprofloxacin under visible light irradiation. *J Colloid Interf Sci* 588:19-30. <https://doi.org/10.1016/j.jcis.2020.12.043>